

Compact Generation of Airy Beams with C-Aperture Metasurface

Eui-Young Song, Gun-Yeal Lee, Hyeonsoo Park, Kyoookun Lee, Joonsoo Kim, Jongwoo Hong, Hwi Kim, and Byounggho Lee*

A novel method to launch finite power Airy beams based on a metasurface is presented. By tailoring the amplitude and phase of the transmitted fields from a metallic C-aperture array, launching Airy beams is achieved in free space. The amplitude and phase of the Airy beam profile can be mapped and tailored by tuning only the tilt angles of the aperture. This structure has multifrequency characteristics, which facilitates Airy beam steering because the trajectory of Airy beams is dependent on the wavelength. In addition, the design method can generate Airy beams which have a very compact main lobe ($\approx 2 \mu\text{m}$). Computational and experimental results show that proposed metasurface can overcome some limitations of the traditional methods to generate Airy beams. The results can be used for potential applications in integrated optics, beam shaping, biosensing, and next-generation holography.

and surface plasmons.^[17–20] Some of these reports showed that the Airy beams can be generated and actively controlled. For example, ballistic motion of Airy beams was controlled using SLM.^[4] In addition, polarization-controllable Airy beams using liquid crystal mask have also been proposed.^[14] However, microsize pixels of the SLM or liquid crystal restrict the design of Airy beams because these require bulky optical system and limit the application for small-scale or integrated beam-shaping devices. Nonlinear generation and manipulation of Airy beams also suffers from long crystal length for making sufficient nonlinear effect.

1. Introduction

In 1978, Berry and Balazs first predicted the nonspreading wave packet from the Schrödinger equation in quantum mechanics for a free particle.^[1] This wave packet is a nontrivial solution of the Schrödinger equation by exploiting the formal analogy between the free-particle Schrödinger equation and the paraxial equation of diffraction. The remarkable features of the Airy packet are nonspreading, freely accelerating, and self-healing ability. In 2007, optical version of the Airy wave packet, called Airy beams, was investigated and observed experimentally by introducing finite-energy Airy beams.^[2,3] Although the generated beam is not ideal Airy packet, the beam still showed all the interesting characteristics of ideal Airy packet: nondiffraction, free-acceleration, and self-healing.

Over the years, Airy waves were generated by various ways including spatial light modulator (SLM),^[4–6] specially designed lens system,^[7,8] nonlinear method,^[9–11] electron,^[12] plasma,^[13] liquid crystal,^[14] surface grating,^[15] subwavelength slit arrays,^[16]

and recently, bulky optical components have started to be replaced by ultrathin and planar elements called metasurfaces. Metasurface is defined as the artificially designed 2D structure which can be made of arrays of sub-wavelength scatterers for arbitrary tuning the characteristics of electromagnetic waves. The scatterers of metasurfaces have a variety of forms such as nanoparticles, apertures, and slits inscribed on the metallic films. Being as thin as only a fraction of the wavelength, the metasurface can change the wavefront of light abruptly. Furthermore, the size of unit cell in metasurface is much less than the wavelength which is an important difference between metasurfaces and conventional optical devices using SLM or liquid crystal. Several metasurfaces were introduced which can modify the wavefront of light by altering its phase, amplitude, and polarization in a desired manner.^[21–40]

In this context, metasurfaces may open new ways to generate and control of Airy beams for compact, integrated optical systems. Recently, multifunctional optical beam shapers based on plasmonic metasurfaces were introduced.^[36] Local polarization and wavelength selectivity of metasurfaces were combined with methods of computer-generated holograms for phase and amplitude modulation. This method successfully demonstrated switching between 1D Airy and Gaussian beams, Hermite–Gaussian beams of different orders, and 2D Airy and Bessel beams. Very recently, second-harmonic Airy beams with tailored beam profiles using nonlinear metasurfaces were introduced.^[41] By tuning both the phase and the amplitude of quadratic nonlinear coefficient locally using computer-generated holograms, nonlinear beam shaping was facilitated. In addition, Airy beam shaping metasurface which consists of the metal nanorods was proposed.^[42] This method used a change of length of the nanorod to control the amplitude of light, and

Dr. E.-Y. Song, G.-Y. Lee, H. Park, K. Lee, Dr. J. Kim, J. Hong, Prof. B. Lee
Inter-University Semiconductor Research Center and School of Electrical
and Computer Engineering
Seoul National University
Gwanak-Gu Gwanakro 1, Seoul 08826, South Korea
E-mail: byounggho@snu.ac.kr

Prof. H. Kim
Department of Electronics and Information Engineering
Korea University
Sejong-ro 2511, Sejong 30019, South Korea

DOI: 10.1002/adom.201601028

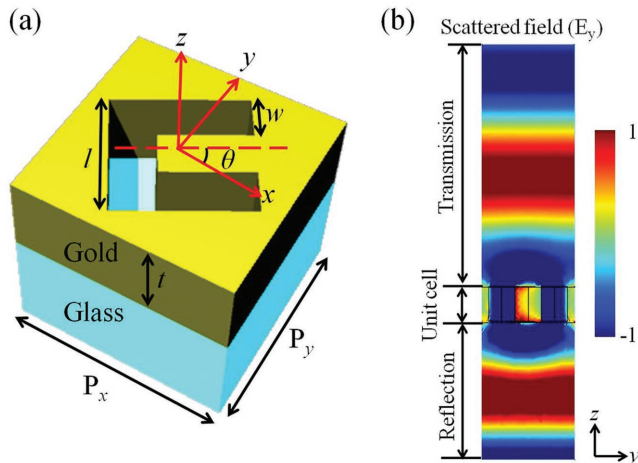


Figure 1. a) Schematics diagram of a proposed unit cell for generation of Airy beam. b) Electric field distribution (E_y) when x -polarized plane wave is backside illuminated.

used an orientation angle of the nanorod to control the phase of light. However, it has a limitation that it only operates on specific and single wavelength because the modulation map is changed by incident wavelength.

In this paper, a novel method for generating and steering of Airy beams based on linear optical metasurface is proposed. To accomplish this, we used C-aperture arrays in which each C-aperture has its own tilt angle. The amplitude and phase of Airy beam profile can be mapped and tailored by tuning only the tilt angles of the C-apertures. Furthermore, the metasurface has multifrequency characteristic in optical regime. This facilitates steering of Airy beams by tuning the wavelength of incident light because the trajectory of Airy beams is a parabolic curve whose curvature is dependent on the wavelength. In comparison to previous approaches for generating and controlling Airy beams, our designing method shows many important merits—ultrathin subwavelength pixel size for compact system, multifrequency characteristic, simple design strategy, and linear optical devices which means that this method is more energy efficient than nonlinear metasurface method. To the best of our knowledge, it is the first realization of Airy beams

having both multifrequency and compact (the size of main lobe: $\approx 2 \mu\text{m}$) characteristics.

2. C-Aperture based Metasurface for Generation of Airy Beam

A schematic diagram of the proposed unit cell for generation of Airy beam is shown in **Figure 1a**. Au film with thickness t is deposited on the glass substrate. C-pattern is inscribed on the Au layer with tilt angle θ about x -axis. The subwavelength periods of this unit cell are P_x and P_y along x and y direction, respectively. When x -polarized plane wave is backside illuminated onto a C-aperture array which has tilt angle θ , the wavefront of transmitted y -polarized light is quasi-plane wave as shown in **Figure 1b**. In addition, its absolute amplitude and phase profiles can be tuned by the tilt angle θ of C-apertures.

Figure 2a,b shows the changes in the relative amplitude and phase of the transmitted y -polarized light at $5 \mu\text{m}$ away from the top of C-aperture. The periods ($P_x = P_y = 400 \text{ nm}$), thickness of Au film ($t = 150 \text{ nm}$), width, and diameter of C-aperture ($w = 80 \text{ nm}$ and $l = 240 \text{ nm}$) are carefully chosen for experimental consideration. In **Figure 2a**, blue curves are four normalized amplitude profiles with $\lambda = 800, 900, 1000,$ and 1100 nm which coincide with each other. These blue curves can be approximated as proportional to $\sin(2\theta)$. **Figure 2b** shows that the phase values of modulated waves are separated by two segments with values near 0 and near π . The deviations from the exact 0 and π get larger as the wavelength gets shorter. In engineering perspective, however, we could approximate the two segments as values of exact 0 and π because the maximum deviation is below 10% . By Babinet principle, these amplitude and phase profiles can be explained in similar ways with V-, C-shaped antennas.^[25,43] We concluded that proposed aperture scatterers show higher energy efficiency than antenna scatterers in our interest range as shown in Part A in the Supporting Information.

In **Figure 3a–d**, y -polarized electric field distributions are shown 20 nm above the C-aperture at selected tilt angles θ . At $\theta = 0^\circ$, an antisymmetric mode about axis of C-aperture is generated. Because this antisymmetric mode is canceled out in far-field region, this explains the dark state at $\theta = 0^\circ$ in

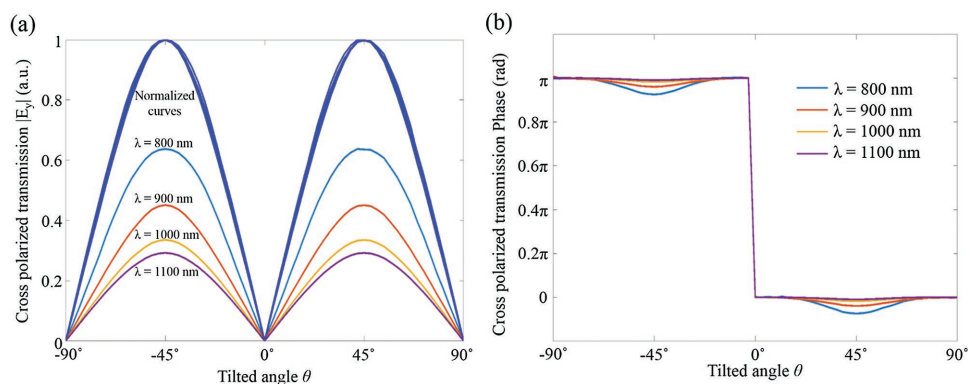


Figure 2. a) Relative amplitude of the transmitted y -polarized light at $5 \mu\text{m}$ away from the top of C-aperture. b) Phase of the transmitted y -polarized light at $5 \mu\text{m}$ away from the top of C-aperture.

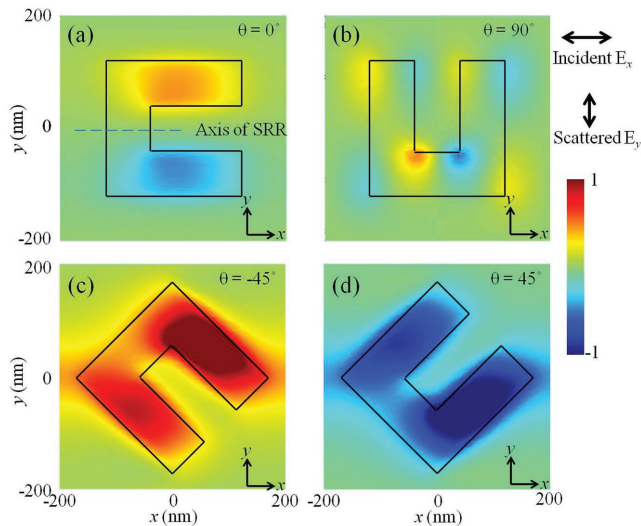


Figure 3. Cross polarized electric field distributions at 20 nm above the C-aperture for a) $\theta = 0^\circ$, b) $\theta = 90^\circ$, c) $\theta = -45^\circ$, and d) $\theta = 45^\circ$.

Figure 2a. At $\theta = 90^\circ$, another antisymmetric mode is generated, which explains the dark state at $\theta = 90^\circ$ in the same way at $\theta = 0^\circ$. At the intermediate state like Figure 3c,d, these two antisymmetric modes simultaneously contribute to the electric field distributions which break antisymmetric distribution of electric field. Because this tendency is robust in the wavelength range of our interest (from $\lambda = 800$ to 1100 nm), the proposed metasurface can be used in multifrequency design.

3. Design of Metasurface for Generation of Airy Beams

We now describe the method of designing metasurface for generating Airy beams. The profile of 1D Airy beam can be expressed as

$$f(x) = \text{Airy}\left(\frac{x}{x_0}\right) \exp\left(a \frac{x}{x_0}\right) \quad (1)$$

The function *Airy* is an Airy function, x_0 is a half width of main lobe, and a is a parameter to obtain Airy beam with finite power. The envelope of the Airy packet represents an oscillating function with alternating positive maxima and negative minima. Therefore, the phase distribution of the Airy function shows alternating segments with values of 0 and π . Proposed unit cell in the previous section can encode the Airy beam profile by sampling Equation (1). Because Equation (1) is 1D equation related with x , the tilt angles of unit cell along y -direction at the same x is identical. **Figure 4** shows the 1D Airy beam profile and its locations of unit cells. At some selected location, a C-aperture with a specific tilt angle was plotted. The parameters of Equation (1) were selected as $x_0 = 1200$ nm and $a = 0.05$. The sampling range is from -20 to $4 \mu\text{m}$. The number of samples is 61, which determines the period of unit cell as 400 nm.

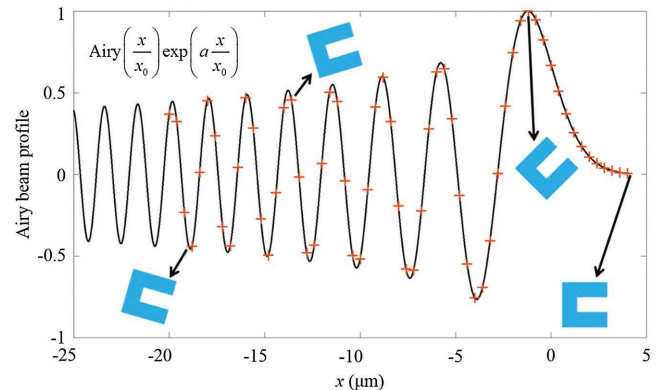


Figure 4. 1D Airy beam profile. The locations of unit cells are marked as “+.” At some selected unit cells, apertures with specific tilt angles were plotted.

There are various points to be considered in designing metasurface. First of all, sampling periods P_x and P_y must be shorter than the operating wavelength to avoid a generation of unexpected diffraction effects. Second, the lower limit of the sampling period is determined by the resolution limit in fabrication although shorter period of sampling guarantees more accurate results. Attachment of neighboring two apertures is another point to consider. Nyquist–Shannon sampling theorem is another limitation which says that more than two samples should be sampled from the one period of the highest frequency component of the desired signal.

After determining the appropriate dimension of the C-aperture and the sampling period with the abovementioned criteria, tilt angles are determined by using Figure 2. Finally, the appropriate shape of the C-aperture array for Airy beam generation is obtained. As long as the restricted aperture size is realistic in fabrication, it is possible to generate Airy beams with the proposed workflow.

4. Compact and Multifrequency Generation of Airy Beams

To verify the validity of the aforementioned design process, we provide some simulations first. To simulate the intensity distribution of the generated 1D Airy beams, a commercial tool (CST Microwave Studio 2016) was employed. The numerical simulations for free space wavelength $\lambda = 750, 800, 900,$ and 1000 nm are presented in **Figure 5a–d**.

Simulation results of the four curves are in good agreement with the blue dashed curves, which are the targeted trajectories of main lobe. Small deviations from the blue dashed curves in the figures are evident as the Airy beams propagate along z axis. We conclude that this small mismatch originates from the finite number of unit cells, which causes the Airy lobes to spread out. This restricts the range of the SPP curves that exactly follow the blue dashed curves. In order to accelerate the Airy lobe more rapidly, it is necessary to substitute the Airy profiles with unit cells on more broad range. In Figure 5a, the side lobes show interference in medium range. This is due to deviation from ideal Airy beam profile as shown in Figure 2 which generates multiple beams at unit cells.

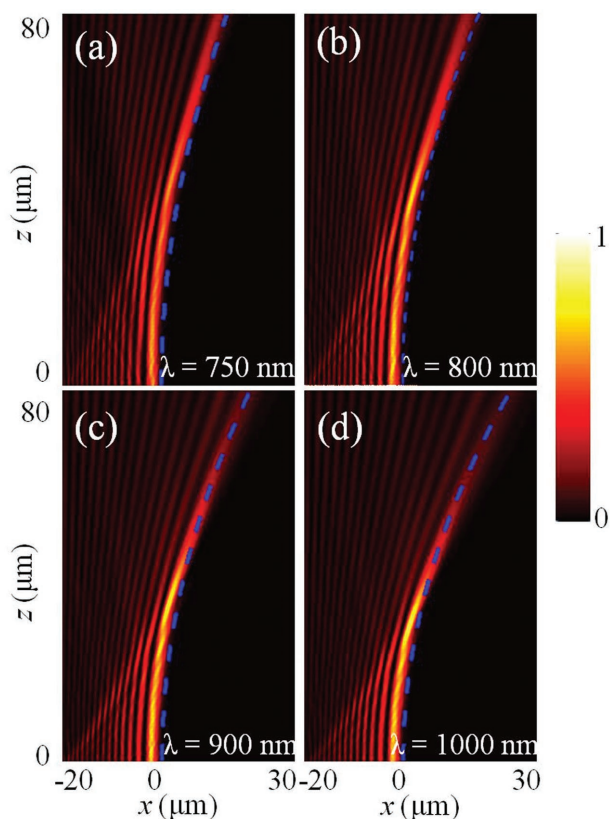


Figure 5. Numerical simulation results for the 1D Airy beams for the free space wavelength a) $\lambda = 750$ nm, b) $\lambda = 800$ nm, c) $\lambda = 900$ nm, and d) $\lambda = 1000$ nm. Blue dashed curves are the targeted trajectories of main lobe.

The multifrequency characteristic of our scheme is an inherent attribution. Because amplitude and phase profile of transmission have approximately constant tendency in the wavelength range of our interest (from $\lambda = 800$ to 1100 nm), we can generate Airy beams with various frequencies on the same structure. This is not the case in many Airy beam generators^[15–20,36,41] because these structures are dependent on wavelength which can generate Airy beam with only one frequency on the same structure. This multifrequency characteristic can be applied to all-optical control of the deflection of Airy beams by relying on the frequency change.

5. Experiment of 2D Airy Beams

To verify the simulation results, we provide some experimental results. The design procedure is identical with that of 1D Airy beams. The profile of 2D Airy beams is as follows which is 2D version of Equation (1)

$$f(x) = \text{Airy}\left(\frac{x}{x_0}\right) \text{Airy}\left(\frac{y}{y_0}\right) \exp\left(a \frac{x}{x_0}\right) \exp\left(a \frac{y}{y_0}\right) \quad (2)$$

The parameters of Equation (2) were selected as $x_0 = 1200$ nm, $y_0 = 1200$ nm, and $a = 0.05$. The unit cells range

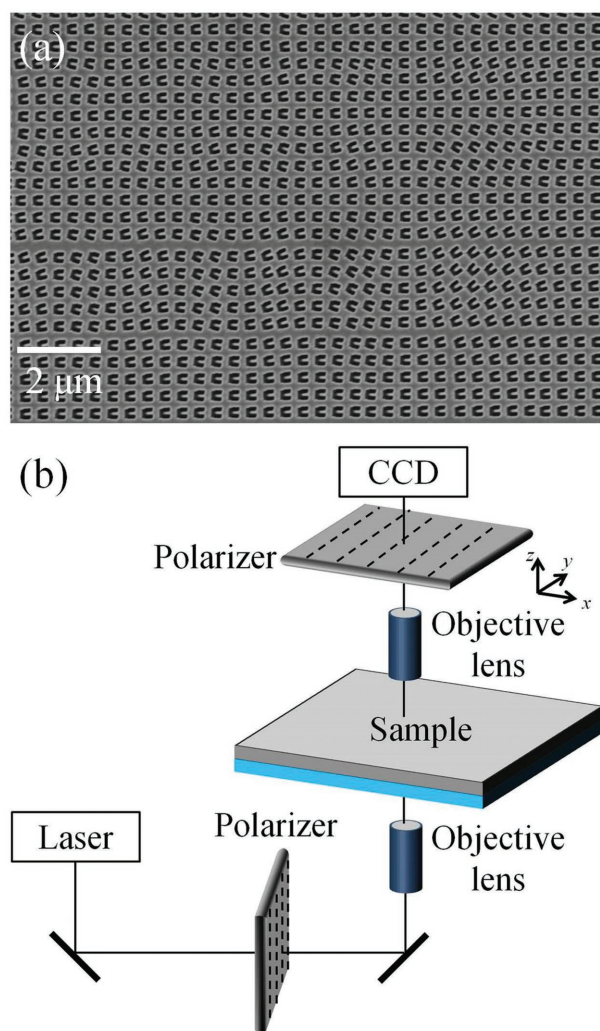


Figure 6. a) FE-SEM images of fabricated sample for 2D Airy beam generation. b) Experimental setup for cross polarized light measurement.

is from -14 to 4 μm for x and y directions. The number of unit cells is 46 by 46 , which determines the period of unit cells as 400 nm along x and y directions.

For sample fabrication, an Au layer with a thickness of 150 nm was evaporated on a fused silica wafer (MUHAN, MHS-1800). Then each C-pattern was inscribed on the Au layer using a focused ion beam (FIB) (FEI, Helios 650). Figure 6a shows the field-enhanced scanning electron microscope (FE-SEM) images of the fabricated sample for generation of Airy beams. According to the image, it is possible to confirm that the size of the fabricated C-pattern is smaller than the unit cells period. The sample was then illuminated from the bottom by the laser with the free-space wavelength of $\lambda = 800$ and 976 nm. The incident light on the sample was polarized with x -direction by linear polarizer. A polarimeter for an infrared source (Thorlabs, PAN5710IR) was used to tune the polarization state of the incident light. By using the oppositely directional polarizer, transmitted light was cross-polarized with y -direction and the generated Airy beam intensity distribution was measured by a charge-coupled device (CCD) camera. Here,

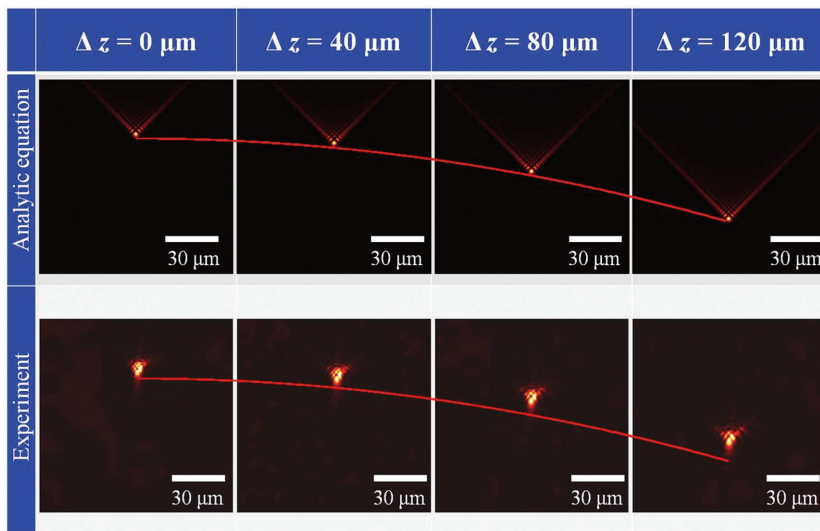


Figure 7. Analytical and experimental results for $z = 0, 40, 80,$ and $120 \mu\text{m}$ at wavelength $\lambda = 800 \text{ nm}$.

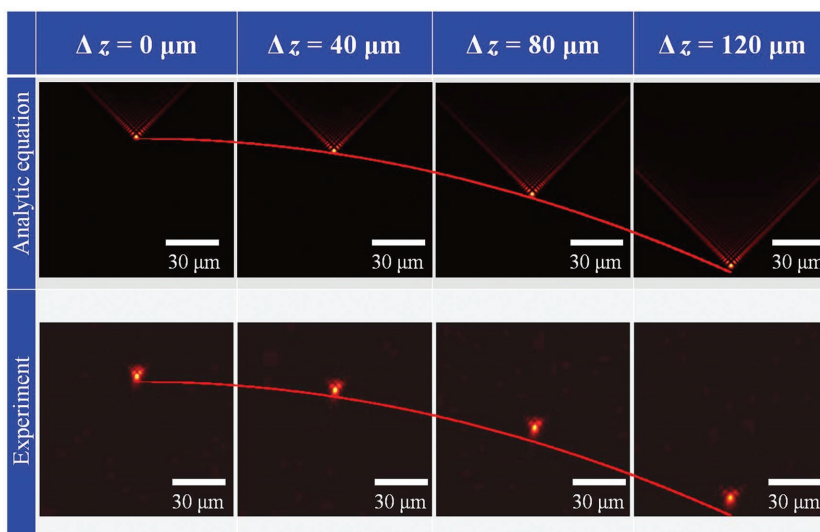


Figure 8. Analytical and experimental results for $z = 0, 40, 80,$ and $120 \mu\text{m}$ at wavelength $\lambda = 976 \text{ nm}$.

a polarizer with high extinction ratio ($>100\,000:1$) was used to reduce the tolerance about the polarization. The experimental setup is shown in Figure 6b.

The experimental results for the 2D Airy beams are presented in **Figures 7 and 8**. In these figures, analytical and experimental results for $z = 0, 40, 80,$ and $120 \mu\text{m}$, at wavelengths $\lambda = 800$ and 976 nm were plotted. Experimental results show some deviation from analytical results. We believe that the finite numerical aperture of the objective lens in the experimental setup might play a role that causes the intensity of the incident light and the incidence angle to be nonuniform. Deflections of Airy beam with respect to z of analytic and experimental results are slightly different from the analytical results. This can be explained as coming from finite number of

samples which restrict the Airy beams from ideal deflection. The efficiency of the metasurface, which is defined as the ratio of the maximum power of the transmitted light to the power of the incident light, is also measured at wavelength $\lambda = 800$ and 976 nm . The experimentally measured efficiencies for the wavelength of 800 and 976 nm are 13.5% and 4.2% , respectively, while those values in simulations are 16.8% and 5% . The difference between the experimental and simulation values is estimated to originate from errors associated with the fabrication of the sample in the FIB milling processes, such as edge blurring of the C-apertures and the tolerances about the polarization of the incident light and the measured light.

6. Conclusion

In conclusion, a novel method for generating and steering of Airy beams with ultrahigh resolution was proposed. To accomplish this, we used C-aperture arrays in which each C-aperture has its own tilt angle. The envelope of the Airy packet represents an oscillating function with alternating positive maxima and negative minima. Therefore, the phase distribution of the Airy function shows alternating segments with values of 0 and π . Proposed unit cell can encode the Airy beam profile by substituting the profile with tilt angles of unit cells. Experimental results show some deviation from analytical results. We believe that the finite numerical aperture of the objective lens in the experimental setup might play a role that causes the intensity of the incident light and the incidence angle to be nonuniform. Deflections of Airy beam with respect to z of analytic and experimental results are slightly different from the analytical results. This can be explained as coming from finite number of samples, which restricts the Airy beams from ideal performance. In comparison to previous approaches for generating and controlling Airy beams, our designing method showed many important merits such as the compactness of the system with subwavelength pixel sizes and the broadband characteristic due to the benefits of metasurfaces and the C-aperture design. We expect that our proposed method of designing Airy beams generation can be employed to excite various types of Airy beams.

Supporting Information

Supporting Information is available from the Wiley Online Library or from the author.

Acknowledgements

E.-Y.S. and G.-Y.L. contributed equally to this work. This work was supported by the Center for Advanced Meta-Materials (CMM) funded by the Ministry of Science, ICT and Future Planning as Global Frontier Project (CMM-2014M3A6B3063710). The authors acknowledge support from the Brain Korea 21 (BK21) project.

Keywords

Airy beams, amplitude and phase modulation, metasurfaces, nondiffraction beams

Received: December 6, 2016
Revised: February 10, 2017
Published online: April 6, 2017

-
- [1] M. V. Berry, N. L. Balazs, *Am. J. Phys.* **1979**, *47*, 264.
 [2] G. A. Siviloglou, J. Broky, A. Dogariu, D. N. Christodoulides, *Phys. Rev. Lett.* **2007**, *99*, 213901.
 [3] G. A. Siviloglou, D. N. Christodoulides, *Opt. Lett.* **2007**, *32*, 979.
 [4] G. A. Siviloglou, J. Broky, A. Dogariu, D. N. Christodoulides, *Opt. Lett.* **2008**, *33*, 207.
 [5] Z. Ren, Q. Wu, Y. Shi, C. Chen, J. Wu, H. Wang, *Opt. Express* **2014**, *20*, 15155.
 [6] J. Broky, G. A. Siviloglou, A. Dogariu, D. N. Christodoulides, *Opt. Express* **2008**, *16*, 12880.
 [7] B. Yalizay, B. Soylu, S. Akturk, *J. Opt. Soc. Am. A* **2010**, *27*, 2344.
 [8] D. G. Papazoglou, S. Suntsov, D. Abdollahpour, S. Tzortzakis, *Phys. Rev. A* **2010**, *81*, 061807.
 [9] T. Ellenbogen, N. V. Bloch, A. G. Padowicz, A. Arie, *Nat. Photonics* **2009**, *3*, 395.
 [10] D. Wei, Y. Yu, M. Cao, L. Zhang, F. Ye, W. Guo, S. Zhang, H. Gao, F. Li, *Opt. Lett.* **2014**, *39*, 4557.
 [11] I. Dolev, T. Ellenbogen, N. V. Bloch, A. Arie, *Appl. Phys. Lett.* **2009**, *95*, 201112.
 [12] N. V. Bloch, Y. Lereah, Y. Lilach, A. Gover, A. Arie, *Nature* **2013**, *494*, 331.
 [13] P. Polynkin, M. Kolesik, J. V. Moloney, G. A. Siviloglou, D. N. Christodoulides, *Science* **2009**, *324*, 229.
 [14] B.-Y. Wei, P. Chen, W. Hu, W. Ji, L.-Y. Zheng, S.-J. Ge, Y. Ming, V. Chigrinov, Y.-Q. Lu, *Sci. Rep.* **2015**, *5*, 17484.
 [15] I. Dolev, I. Epstein, A. Arie, *Phys. Rev. Lett.* **2012**, *109*, 203903.
 [16] D. Choi, Y. Lim, I.-M. Lee, S. Roh, B. Lee, *IEEE Photonics Technol. Lett.* **2012**, *24*, 1440.
 [17] L. Li, T. Li, S. M. Wang, C. Zhang, S. N. Zhu, *Phys. Rev. Lett.* **2011**, *107*, 126804.
 [18] P. Zhang, S. Wang, Y. Liu, X. Yin, C. Lu, Z. Chen, X. Zhang, *Opt. Lett.* **2011**, *36*, 3191.
 [19] A. Minovich, A. E. Klein, N. Janunts, T. Pertsch, D. N. Neshev, Y. S. Kivshar, *Phys. Rev. Lett.* **2011**, *107*, 116802.
 [20] N. Meinzer, W. L. Brnes, I. R. Hooper, *Nat. Photonics* **2010**, *8*, 889.
 [21] N. Yu, F. Capasso, *Nat. Mater.* **2014**, *13*, 139.
 [22] D. Lin, P. Fan, E. Hasman, M. L. Brongersma, *Science* **2014**, *345*, 298.
 [23] A. Pors, G. M. Nielsen, R. L. Eriksen, S. I. Bozhevolnyi, *Nano Lett.* **2013**, *13*, 829.
 [24] X. Ni, A. V. Kildishev, V. M. Shalaev, *Nat. Commun.* **2013**, *4*, 2807.
 [25] N. Yu, P. Genevet, M. A. Kats, F. Aieta, J.-P. Tetienne, F. Capasso, Z. Gaburro, *Science* **2011**, *334*, 333.
 [26] L. Huang, X. Chen, H. Mühlenbernd, H. Zhang, S. Chen, B. Bai, Q. Tan, G. Jin, K.-W. Cheah, C.-W. Qiu, J. Li, T. Zentgraf, S. Zhang, *Nat. Commun.* **2013**, *4*, 2808.
 [27] X. Yin, Z. Ye, J. Rho, Y. Wang, X. Zhang, *Science* **2013**, *339*, 1405.
 [28] J. Lee, M. Tymchenko, C. Argyropoulos, P.-Y. Chen, F. Lu, F. Demmerle, G. Boehm, M.-C. Amann, A. Alù, M. A. Belkin, *Nature* **2014**, *511*, 65.
 [29] A. V. Kildishev, A. Boltasseva, V. M. Shalaev, *Science* **2013**, *339*, 1232009.
 [30] X. Ni, S. Ishii, A. V. Kildishev, V. M. Shalaev, *Light Sci. Appl.* **2013**, *2*, e72.
 [31] Y. Zhao, M. A. Belkin, A. Alù, *Nat. Commun.* **2012**, *3*, 870.
 [32] Y. Zhao, A. Alù, *Phys. Rev. B* **2011**, *84*, 205428.
 [33] M. Kang, T. H. Feng, H. T. Wang, J. S. Li, *Opt. Express* **2012**, *20*, 15882.
 [34] S. Sun, Q. He, S. Xiao, Q. Xu, X. Li, L. Zhou, *Nat. Mater.* **2012**, *11*, 426.
 [35] X. Ni, N. K. Emani, A. V. Kildishev, A. Boltasseva, V. M. Shalaev, *Science* **2012**, *335*, 427.
 [36] O. Avayu, O. Eisenbach, R. Ditzovski, T. Ellenbogen, *Opt. Lett.* **2014**, *39*, 3892.
 [37] Z. Li, H. Cheng, Z. Liu, S. Chen, J. Tian, *Adv. Opt. Mater.* **2016**, *4*, 1230.
 [38] L. Cong, Y. K. Srivastava, R. Singh, *Adv. Opt. Mater.* **2016**, *4*, 848.
 [39] L. Cong, P. Pitchappa, Y. Wu, L. Ke, C. Lee, N. Singh, H. Yang, R. Singh, *Adv. Opt. Mater.* **2017**, *5*, 1600716.
 [40] L. Cong, Y. K. Srivastava, R. Singh, *Appl. Phys. Lett.* **2016**, *108*, 011110.
 [41] S. K. Zur, O. Avayu, L. Michaeli, T. Ellenbogen, *ACS Photonics* **2016**, *3*, 117.
 [42] Z. Li, H. Cheng, Z. Liu, S. Chen, J. Tian, *Adv. Opt. Mater.* **2016**, *4*, 1230.
 [43] L. Liu, X. Zhang, M. Kenney, X. Su, N. Xu, C. Ouyang, Y. Shi, J. Han, W. Zhang, S. Zhang, *Adv. Mater.* **2014**, *26*, 5031.